J. Phase Equilib. Diffus.
https://doi.org/10.1007/s11669-023-01026-2

Liquidus Projection of the Al-Ta-V System

D. A. de Abreu[1,2] · **D. F. Barros**[2] · **J. C. P. Santos**[2,3,6] · **K. E. Borowski**[2] ·
A. A. A. P. da Silva[4] · **N. Chaia**[5] · **C. A. Nunes**[2] · **G. C. Coelho**[2]

Submitted: 7 November 2022 / in revised form: 16 December 2022 / Accepted: 19 December 2022

Abstract Phase equilibria in the Al-Ta-V system have an important role for designing Al-containing refractory multiprincipal element alloys. In order to improve the available data related to this system and contribute to the development of alloys with good microstructural stability and oxidation resistance, the *liquidus* projection of the Al-Ta-V system is reported for the first time in the present work. The experimental investigations were carried out via microstructural characterization of thirty-one as-cast alloys using scanning electron microscopy (SEM), energy dispersive spectroscopy (EDS) and x-ray diffractometry (XRD). The primary solidification field of BCC is preponderant in relation to those of the other phases. No microstructural signs of phase separation were observed between the isostructural VAl_3 and (ε)-$TaAl_3$ phases, which suggest a $MeAl_3$ solid solution connecting the Al-Ta and Al-V binary edges. Alloys in all of the primary solidification fields up to 85 at.% (BCC, σ, $Ta_{39}Al_{69}$, V_5Al_8, $MeAl_3$) were experimentally produced. Two class II and one type III ternary invariant reactions are suggested based on experimental data: (U_I) $Liq + \sigma \leftrightarrow BCC + Ta_{39}Al_{69}$, (U_{II}) $Liq + Ta_{39}Al_{69} \leftrightarrow V_5Al_8 + MeAl_3$ and (P_I) $Liq + BCC + V_5Al_8 \leftrightarrow Ta_{39}Al_{69}$. Ternary invariant reactions near to the Al-rich corner are suggested based on extrapolated thermodynamic data. The reported ternary compound τ-$Al_{35-48}Ta_{32-42}V_{17-30}$ was not observed in the microstructures of the as-cast alloys obtained in the present work, suggesting that its formation occurs from a solid-state reaction.

Keywords Al-Ta-V system · as-cast alloys · *liquidus* projection · solid-liquid phase equilibria projection · solid-liquid phase equilibria

1 Introduction

Multiprincipal element alloys (MEAs), also called high entropy alloys (HEAs) are potential materials to be used as structural components at high temperature applications, especially those constituted by refractory metals.[1,2] In this context, several research groups are investigating refractory multiprincipal element alloys (RMEAs) with Al addition, in order to obtain low density alloys with good oxidation resistance.[3–6] In this context, the study of the phase equilibria in ternary systems involving refractory metals and Al is important,[7–11] since the use of these data, along with thermodynamic information and computational tools allows the design of alloys with single-phase

---

✉ D. A. de Abreu
Danilo-Alencar.De-Abreu@iww.tu-freiberg.de

✉ J. C. P. Santos
jcpsantos@northwestern.edu

[1] Institute of Materials Science, TU Bergakademie Freiberg, Gustav-Zeuner Straße 5, 09599 Freiberg, Saxony, Germany

[2] Lorena School of Engineering, University of São Paulo, Polo Urbo-Industrial Gleba AI-6, Lorena, São Paulo 12602-810, Brazil

[3] Center of Hierarchical Materials Design (CHiMaD), Northwestern University, 2205 Tech Drive, Evanston, IL 60208

[4] Institute of Mechanical Engineering, Federal University of Itajubá, Av. B P S, 1303, Itajubá, Minas Gerais 37500-903, Brazil

[5] Institute of Science and Technology, Federal University of Alfenas, Rod. José Aurélio Varela, 11999, Poços de Caldas, Minas Gerais 37715-400, Brazil

[6] Northwestern University and the National Institute of Standards and Technology (NIST), Evanston

microstructures.[12–15] Considering the multicomponent system Al-Cr-Nb-Ta-Ti-V-Zr, a careful review of the literature indicated some ternary subsystems with little or no information available, such as the Al-Ta-V system, for which no *liquidus* projection had been reported until now. In the present work, the experimental *liquidus* projection for the Al-Ta-V system is reported based on microstructural characterization of thirty-one arc-melted as-cast alloys.

2 Literature Review

2.1 Binary Systems

The Al-V system was experimentally investigated by several authors[16–19] and the results reported for this system up to 1989 were summarized by Murray.[20] Saunders[21] performed the first thermodynamic assessment of this system. More recently, a paper published by Richter and Ipser[22] presented an enhanced version of the aluminum rich part of the Al-V system (between 0 and 50 at.% of V). Based on the experimental results obtained from Richter and Ipser,[22] three other thermodynamic assessments were performed by Gong et al.,[23] Lindhal et al.[24] and Kroupa et al.[25] Five intermetallic compounds (VAl_3, V_5Al_8, V_2Al_{21}, V_4Al_{23} and V_7Al_{45}) are stable in Al-V system, all being formed by peritectic reactions.

Danon and Cervant[26] performed an assessment to describe the phase equilibria in Ta-V system, using experimental results obtained by Eremenko et al.,[27] Nefedov et al.[28] and Savitskii and Efimov.[29] Danon and Cervant[26] reported the stability of C14 phase at high temperatures up to 1702K, while the C15 phase is stable up to 1548K. Recently, Pavlů et al.[30] suggested that the C14 phase can be also stable at lower temperatures based on ab-initio calculations.

The Al-Ta system was calculated by Du and Fetzer[31] using experimental data from Subramanian et al.[32] and Mahne et al.[33] However, the thermodynamic assessment was not consistent with the experimental data obtained by Nowotny and Neckel[34] on one side, and Meschel and Kleppa[35] on the other side, which resulted in inconsistent solid state transformations from the calculations.

Recently, Witusiewicz et al.[36] performed a new thermodynamic assessment using the previous literature data and their own experimental data obtained from heat-treated and as-cast alloys. Three intermetallic compounds (ε)-$TaAl_3$, σ and $Ta_{39}Al_{69}$ are formed from peritectic reactions, while φ phase is formed congruently from the σ phase.

Figure 1 shows the most recent thermodynamic assessments of the binary edges associated to the Al-Ta-V system, calculated with the thermodynamic parameters from Kroupa et al.[25] for the Al-V system; Pavlů et al.[30] for the Ta-V system and Witusiewicz et al.[36] for the Al-Ta system. These calculated phase diagrams were used to support the analysis and customize the figures and tables of the present work. The crystallographic data[37] of the stable phases are presented in Table 1 and the invariant reactions from the binary systems are found in Table 2.

2.2 Al-Ta-V Ternary System

Raman[38] reported an experimental isothermal section for the Al-Ta-V system at 1273 K as shown in Fig. 2(a), based on heat-treated samples characterized by x-ray diffraction (XRD). The authors observed a ternary compound, with approximated stochiometry of Ta_2VAl_3 and a significant range of stability. Bochvar[[39] performed a new evaluation of the phase equilibria reported by Raman,[38] as shown in Fig. 2(b). Although no additional experimental data was obtained by Bochvar,[39] the solubility limits of the single-phase regions were better adjusted.

Both authors[38,39] did not consider the stability of the C15 and ϕ phases on the Ta-V and the Al-Ta sides, respectively, for these isothermal sections at 1273 K, which is inconsistent with the binary systems shown in Fig. 1(b) and (c). Besides that, Raman and Bochvar[38,39] considered the stability of the Ta_2Al_3 phase, which is inconsistent with the experimental results obtained by Witusiewicz et al.[36] for the Al-Ta system. Furthermore, phase separation between the isostructural $D0_{22}$ compounds VAl_3 and (ε)-$TaAl_3$ (see Table 1 for more details) was suggested without experimental data. Thus, as far as we know, the phase equilibria in the Al-Ta-V ternary system are not well established.

The composition interval and the crystallographic data of the ternary compound (also called τ-$Al_{35-48}Ta_{32-42}V_{17-30}$) observed by Raman[38] were recently obtained by Harbrecht et al.[40]. The crystallographic data of this pentagonal antiprismatic columnar structure is indicated with an asterisk symbol in Table 1. These authors indicated that this compound is stable only for temperatures lower than 1473K, forming from BCC in a solid-state reaction.

3 Experimental Procedure

Thirty-one as-cast alloys were prepared from high purity elements Al (min. 99.96 wt.%), Ta (min. 99.8 wt.%) and V (min. 99.7 wt.%). Ingots of 2 g were arc-melted under argon atmosphere (min. 99.995%) in a water-cooled copper crucible. The alloys were melted five times and flipped after each melting step to obtain chemically homogeneous

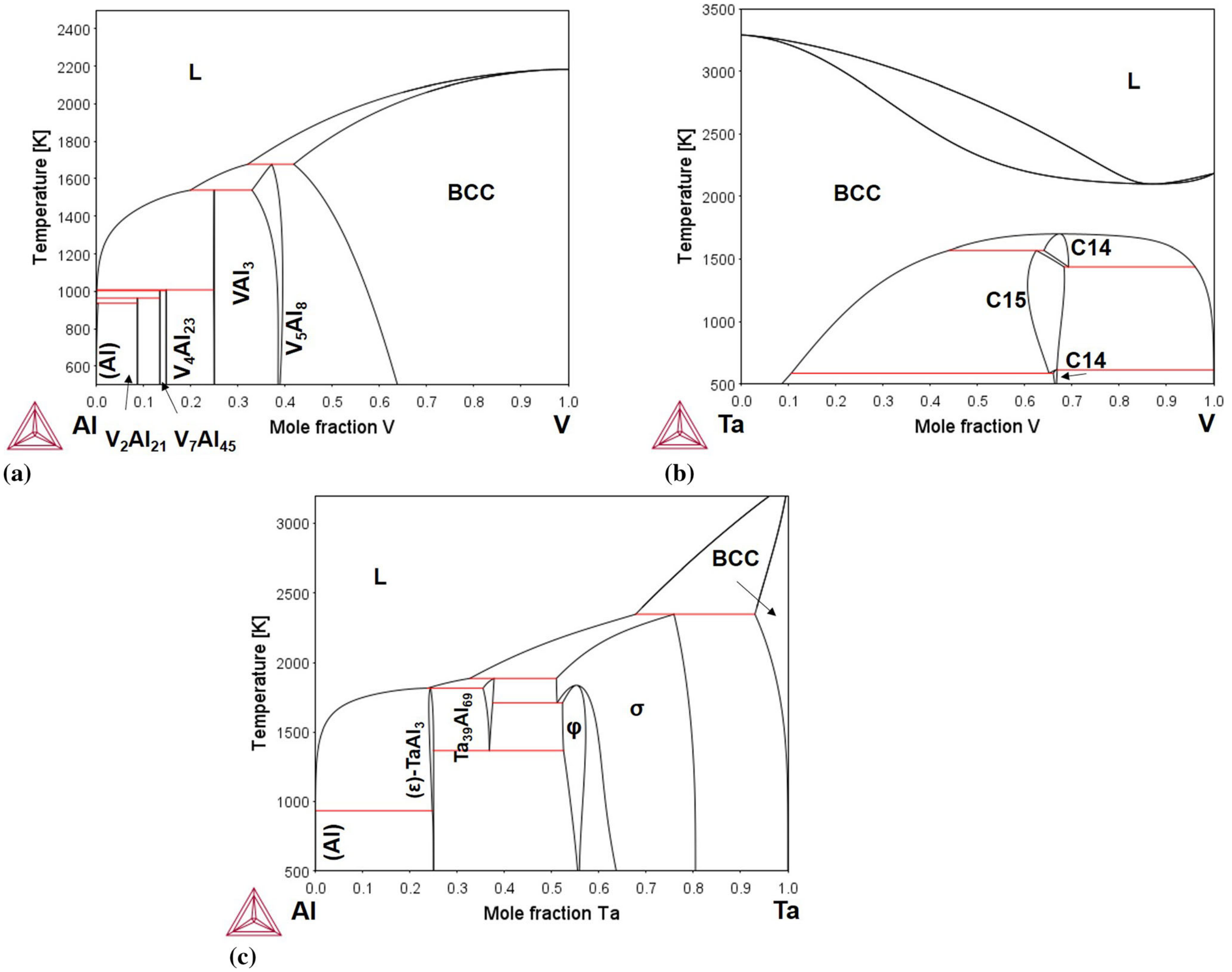

Fig. 1 Binary phase diagrams that composes the Al-Ta-V system: (a) Al-V system,[25] (b) Ta-V system[30] and (c) Al-Ta system[36]

Table 1 Crystallographic data of the solid phases in the Al-Ta-V system[37]

Phase	Pearson symbol	Space group	Prototype	Strukturbericht designation
(Al)	$cF4$	$Fm\bar{3}m$	Cu	$A1$
BCC	$cI2$	$Im\bar{3}m$	W	$A2$
V_5Al_8	$cI52$	$I\bar{4}3m$	Cu_5Zn_8	$D8_2$
VAl_3	$tI8$	$I4/mmm$	$TiAl_3$	$D0_{22}$
V_4Al_{23}	$hP54$	$P6_3/mmc$	V_4Al_{23}	.
V_7Al_{45}	$mC104$	$C2/m$	V_7Al_{45}	.
V_2Al_{21}	$cF176$	$Fd\bar{3}m$	VAl_{10}	.
σ	$tP30$	$P4_2/mnm$	σ-FeCr	$D8_b$
φ	$mP86$	$P2_1/c$	$Ta_{48}Al_{38}$	.
$Ta_{39}Al_{69}$	$cF432$	$F\bar{4}3m$	$Ta_{39}Al_{69}$	.
(ε)-$TaAl_3$	$tI8$	$I4/mmm$	$TiAl_3$	$D0_{22}$
C14	$hP12$	$P6_3/mmc$	$MgZn_2$	$C14$
C15	$cF24$	$Fd\bar{3}m$	$MgCu_2$	$C15$
*τ-$Al_{35-48}Ta_{32-42}V_{17-30}$	$oC28$	$Cmca$	.	.

*Ternary phase.

Table 2 Invariant reactions involving liquid phase from binary systems[25,30,36]

Invariant reaction	Identification	Type	Liquid composition	Temp., K	Ref.
Liq. + BCC ↔ σ	p^1	Peritectic	75.9 at.% Ta	2347	Al-Ta system[36]
Liq. ↔ BCC	c^1	Congruent	12.0 at.% Ta	2114	Ta-V system[30]
Liq. + σ ↔ $Ta_{39}Al_{69}$	p^2	Peritectic	37.8 at.% Ta	1885	Al-Ta system[36]
Liq. + $Ta_{39}Al_{69}$ ↔ (ε)-$TaAl_3$	p^3	Peritectic	24.4 at.% Ta	1814	Al-Ta system[36]
Liq. + BCC ↔ V_5Al_8	p^4	Peritectic	34.8 at.% V	1680	Al-V system[25]
Liq. + V_5Al_8 ↔ VAl_3	p^5	Peritectic	20.5 at.% V	1542	Al-V system[25]
Liq. + VAl_3 ↔ V_4Al_{23}	p^6	Peritectic	< 1.0 at.% V	1009	Al-V system[25]
Liq. + V_4Al_{23} ↔ V_7Al_{45}	p^7	Peritectic	< 1.0 at.% V	1002	Al-V system[25]
Liq. + V_7Al_{45} ↔ V_2Al_{21}	p^8	Peritectic	< 1.0 at.% V	963	Al-V system[25]
Liq. + V_2Al_{21} ↔ (Al)-FCC	p^9	Peritectic	< 1.0 at.% V	936	Al-V system[25]
Liq. + (ε-$TaAl_3$) ↔ (Al)	p^{10}	Peritectic	< 1.0 at.% Ta	933	Al-Ta system[36]

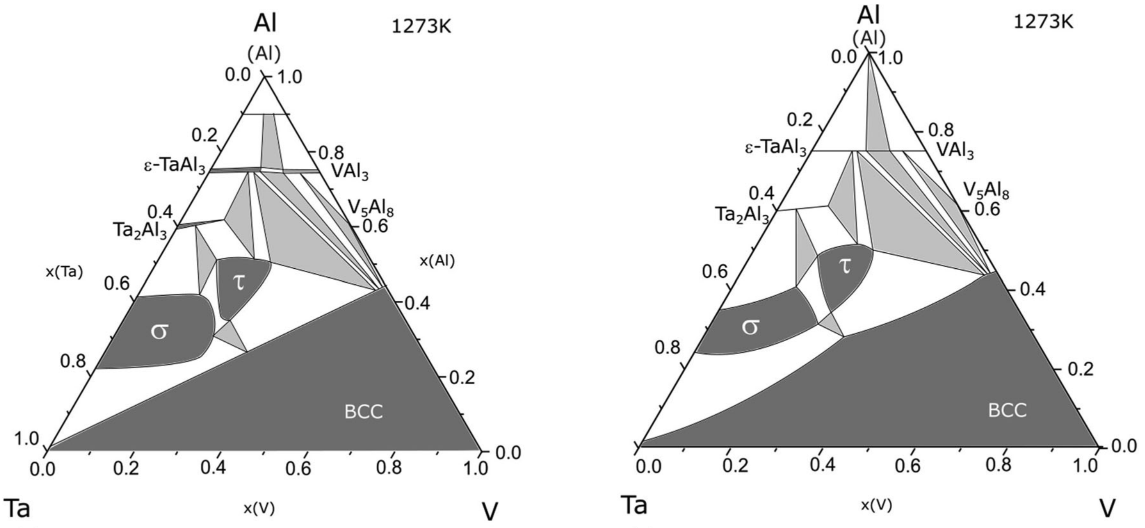

(a) **(b)**

Fig. 2 Isothermal sections of the Al-Ta-V system at 1273 K: (a) Raman[38] and (b) Bochvar[39]

samples. Mass losses during the melting process did not exceeded 0.95 wt.%. The metallographic preparation was performed according to the following procedure: the samples were hot-mounted in epoxy resin, ground with SiC abrasive paper (P320 up to P2400), polished with colloidal silica (0.05 μm), cleaned with ethanol and dried with hot air.

The microstructural characterization of the as-cast alloys was performed using a HITACHI-TM3000 scanning electron microscope (SEM) in the backscattered electrons mode (BSE). The global and the phases chemical compositions were obtained by energy dispersive x-ray spectroscopy (EDS) using a Swift ED-3000 system from Oxford instruments, to guide our microstructural interpretations.

The phases present in each sample were also determined by x-ray diffractometry (XRD) characterization in a Panalytical Empyrean diffractometer using Cu-k_α radiation, scanning angle 2θ in the 10°-90° range with a step size of 0.02° and 50 s counting time. ICSD (Inorganic Crystal Structure Database, 2017) data[37] were used for interpretation of the powder diffraction patterns. Qualitative and quantitative analyses of the XRD patterns were performed by Rietveld analysis using Topas software (Bruker).

4 Results and Discussion

Table 3 gives the nominal composition of the alloys and their respective mass losses resulting from the arc-melting process. These mass losses did not exceed 1 wt.%, indicating a very small deviation from the nominal

Table 3 Nominal compositions of as-cast alloys and phases identified by SEM/XRD with their respective volume fractions and cell parameters

ID.	Nominal composition			Mass losses	Possible composition interval			Phase	Vol., %	Cell parameters, Å
	Al, at.%	Ta, at.%	V, at.%	wt.%	Al, at.%	Ta, at.%	V, at.%			
#1	38.0	40.0	22.0	0.49	36.9-38.3	39.9-40.1	21.3-22.4	BCC*	100.0	$a = 3.1839$
#2	35.0	40.0	25.0	0.91	32.9-35.6	39.7-41.3	23.7-25.8	BCC*	100.0	$a = 3.1775$
#3	35.0	30.0	35.0	0.67	33.7-35.4	29.7-30.6	34.3-35.7	BCC*	100.0	$a = 3.1554$
#4	45.0	15.0	40.0	0.73	44.1-45.4	14.8-15.2	39.5-40.6	BCC*	100.0	$a = 3.1214$
#5	51.0	11.0	38.0	0.06	51.0-51.1	11.0-11.0	37.9-38.0	BCC*	100.0	$a = 3.0504$
#6	57.0	6.0	37.0	0.95	56.3-57.5	5.8-6.1	36.4-37.6	BCC*	31.2	$a = 3.0963$
								V_5Al_8	68.8	$a = 9.2577$
#7	45.0	50.0	5.0	0.04	45.0-45.1	49.9-50.0	4.9-5.0	σ*	82.8	$a = 9.7643/c = 5.2080$
								$Ta_{39}Al_{69}$	17.2	$a = 19.1714$
#8	40.0	35.0	25.0	0.51	38.9-40.3	34.9-35.6	24.4-25.5	BCC*	100.0	3.1673
#9	40.0	25.0	35.0	0.52	39.2-40.4	24.8-25.3	34.5-35.5	BCC*	100.0	3.1443
#10	50.0	38.0	12.0	0.84	48.6-50.8	37.7-39.1	10.7-12.3	σ*	10.5	$a = 9.7756/c = 5.1571$
								BCC	6.0	$a = 3.2989$
								$Ta_{39}Al_{69}$	59.5	$a = 19.1773$
#11	50.0	30.0	20.0	0.06	49.9-50.1	30.0-30.1	19.9-20.0	BCC	9.4	3.1299
								$Ta_{39}Al_{69}$	90.6	$a = 19.1313$
#12	48.0	21.0	31.0	0.40	47.1-48.4	20.8-21.3	30.4-31.5	BCC*	100.0	3.1385
#13	60.0	20.0	20.0	0.87	59.6-60.3	19.9-20.2	19.6-20.2	$Ta_{39}Al_{69}$ (i)*	38.7	$a = 18.7538$
								$Ta_{39}Al_{69}$ (ii)	22.5	$a = 19.0372$
								BCC	38.8	$a = 3.1249$
#14	60.0	35.0	5.0	0.26	59.0-60.9	34.7-35.9	3.7-5.1	σ*	10.4	$a = 9.7756/c = 5.0789$
								$Ta_{39}Al_{69}$	48.3	$a = 19.1744$
								$MeAl_3$	41.3	$a = 3.6654/c = 8.3512$
#15	58.0	12.0	30.0	0.34	57.8-58.1	11.9-12.1	29.8-30.2	$Ta_{39}Al_{69}$*	100.0	$a = 18.6378$
#16	65.0	4.0	31.0	0.35	64.8-65.2	3.9-4.0	30.8-31.2	$Ta_{39}Al_{69}$*	79.4	$a = 19.1303$
								$MeAl_3$	20.6	$a = 3.8344/c = 8.4965$
#17	70.0	20.0	10.0	0.34	69.6-70.5	19.8-20.3	9.4-10.1	$MeAl_3$*	57.3	$a = 3.8356/c = 8.5027$
								V_5Al_8	42.7	$a = 9.3169$
#18	66.0	14.0	20.0	0.35	65.7-66.2	13.9-14.1	19.7-20.2	$Ta_{39}Al_{69}$*	4.9	$a = 18.6670$
								$MeAl_3$	30.3	$a = 3.8224/c = 8.4569$
								V_5Al_8	64.8	$a = 9.3169$
#19	67.0	6.0	27.0	0.18	66.9-67.1	6.0-6.0	16.9-27.0	$MeAl_3$*	57.9	$a = 3.7989/c = 8.3769$
								V_5Al_8	42.1	$a = 9.2673$
#20	72.0	4.0	24.0	0.61	71.8-72.4	3.9-4.0	23.6-24.2	$MeAl_3$*	98.1	$a = 3.7888/c = 8.3507$
								(Al)	1.9	$a = 4.0445$
#21	70.0	10.0	20.0	0.31	69.8-70.2	9.9-10.0	19.8-20.1	$MeAl_3$*	74.0	$a = 3.8115/c = 8.4308$
								V_5Al_8	26.0	$a = 9.2651$
#22	75.0	15.0	10.0	0.15	74.9-75.1	14.9-15.1	9.9-10.0	$MeAl_3$*	100.0	$a = 3.8254/c = 8.4816$
#23	80.0	10.0	10.0	0.22	79.9-80.1	9.9-10.0	9.8-10.0	$MeAl_3$*	93.3	$a = 3.8159/c = 8.4537$
								(Al)	6.6	$a = 4.0449$
#24	80.0	3.0	17.0	0.12	80.0-80.1	3.0-3.0	16.9-17.0	$MeAl_3$*	92.4	$a = 3.7908/c = 8.3628$
								(Al)	7.6	$a = 4.0474$
#25	62.0	28.0	10.0	0.52	61.5-62.5	27.8-28.4	9.4-10.2	V_5Al_8*	71.4	9.2760
								$MeAl_3$	28.6	$a = 3.7918/c = 8.3531$
#26	40.0	45.0	15.0	0.17	39.8-40.4	44.8-15.1	14.6-15.0	σ*	100.0	$a = 9.7895/c = 5.1139$
#27	55.0	30.0	15.0	0.64	54.3-55.6	29.7-30.5	14.1-15.2	$Ta_{39}Al_{69}$ (i)*	87.2	$a = 19.1106$

Table 3 continued

ID.	Nominal composition			Mass losses	Possible composition interval			Phase	Vol., %	Cell parameters, Å
	Al, at.%	Ta, at.%	V, at.%	wt.%	Al, at.%	Ta, at.%	V, at.%			
								$Ta_{39}Al_{69}$ (ii)	5.7	$a = 18.7041$
								BCC	7.1	$a = 3.1369$
#28	55.0	20.0	25.0	0.43	54.5-55.2	19.8-20.2	24.7-25.3	$Ta_{39}Al_{69}$ (i)*	9.2	$a = 18.7410$
								$Ta_{39}Al_{69}$ (i)i	43.2	$a = 19.1067$
								BCC	47.6	$a = 3.1438$
#29	57.0	26.0	17.0	0.37	56.6-57.3	25.9-26.2	16.6-17.2	$Ta_{39}Al_{69}$ (i)*	79.5	$a = 19.0926$
								$Ta_{39}Al_{69}$ (ii)	7.2	$a = 18.7680$
								BCC	13.3	$a = 3.1104$
#30	35.0	55.0	10.0	0.09	34.9-35.2	54.9-55.1	9.8-10.0	σ*	100.0	$a = 9.8141/c = 5.1605$
#31	54.0	12.0	34.0	0.26	53.7-54.1	11.9-12.1	33.9-34.2	$Ta_{39}Al_{69}$ (i)*	13.1	$a = 18.6247$
								$Ta_{39}Al_{69}$ (ii)	13.1	$a = 19.0503$
								BCC	73.8	$a = 3.1163$

*Primary phase.

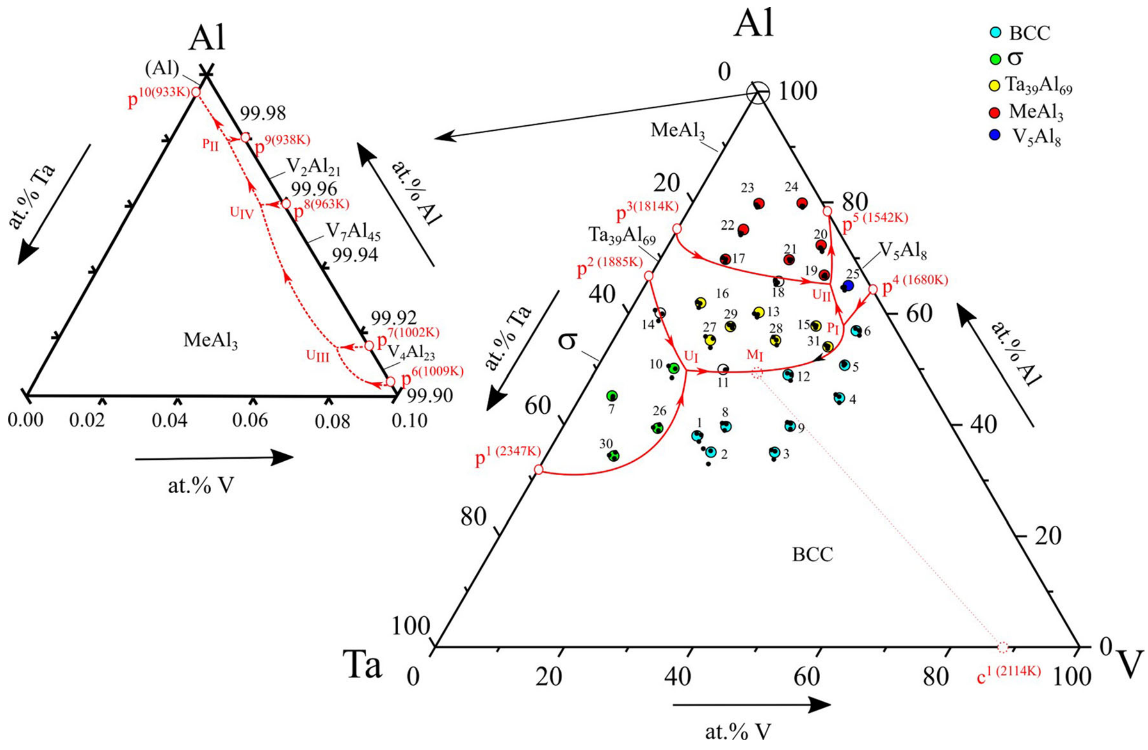

Fig. 3 *Liquidus* projection of Al-Ta-V system reported in this work. The continuous and dashed lines represent the monovariant lines that were determined experimentally or by thermodynamic calculation, respectively[25,30,36]

composition. The possible composition intervals were then calculated by assigning the observed mass loss to each of the elements, resulting in maximum and minimum values, as indicated in Table 3. The observed phases for each alloy are listed, as well as their respective volume fractions and cell parameters obtained from refinement using the Rietveld analyses. The primary phase is marked with an asterisk symbol.

The experimental *liquidus* projection reported for the Al-Ta-V system is shown in Fig. 3. The nominal compositions of the samples were plotted using different symbols for the different primary phases identified in each alloy. Three small black circles are also plotted in Fig. 3 denoting

Table 4 Reported ternary invariant reactions of the Al-Ta-V system involving the liquid phase

Ternary invariant reaction	ID	Estimated liquid composition		
		Al, at.%	Ta, at.%	V, at.%
Liq. + $\sigma \leftrightarrow$ BCC + $Ta_{39}Al_{69}$	U_I	50.0	36.0	14.0
Liq. + BCC + $V_5Al_8 \leftrightarrow Ta_{39}Al_{69}$	P_I	57.0	8.0	35.0
Liq + $Ta_{39}Al_{69} \leftrightarrow MeAl_3 + V_5Al_8$	U_{II}	66.0	7.0	27.0
*Liq + $V_4Al_{23} \leftrightarrow MeAl_3 + V_5Al_{47}$	U_{III}	99.92	0.02	0.06
*Liq + $V_7Al_{45} \leftrightarrow V_2Al_{21} + MeAl_3$	U_{IV}	99.96	0.01	0.02
*Liq + $V_2Al_{21} + MeAl_3 \leftrightarrow$ (Al)	P_{II}	99.98	0.01	0.01

*Reactions suggested based on extrapolated data from Ref [25, 30, 36]

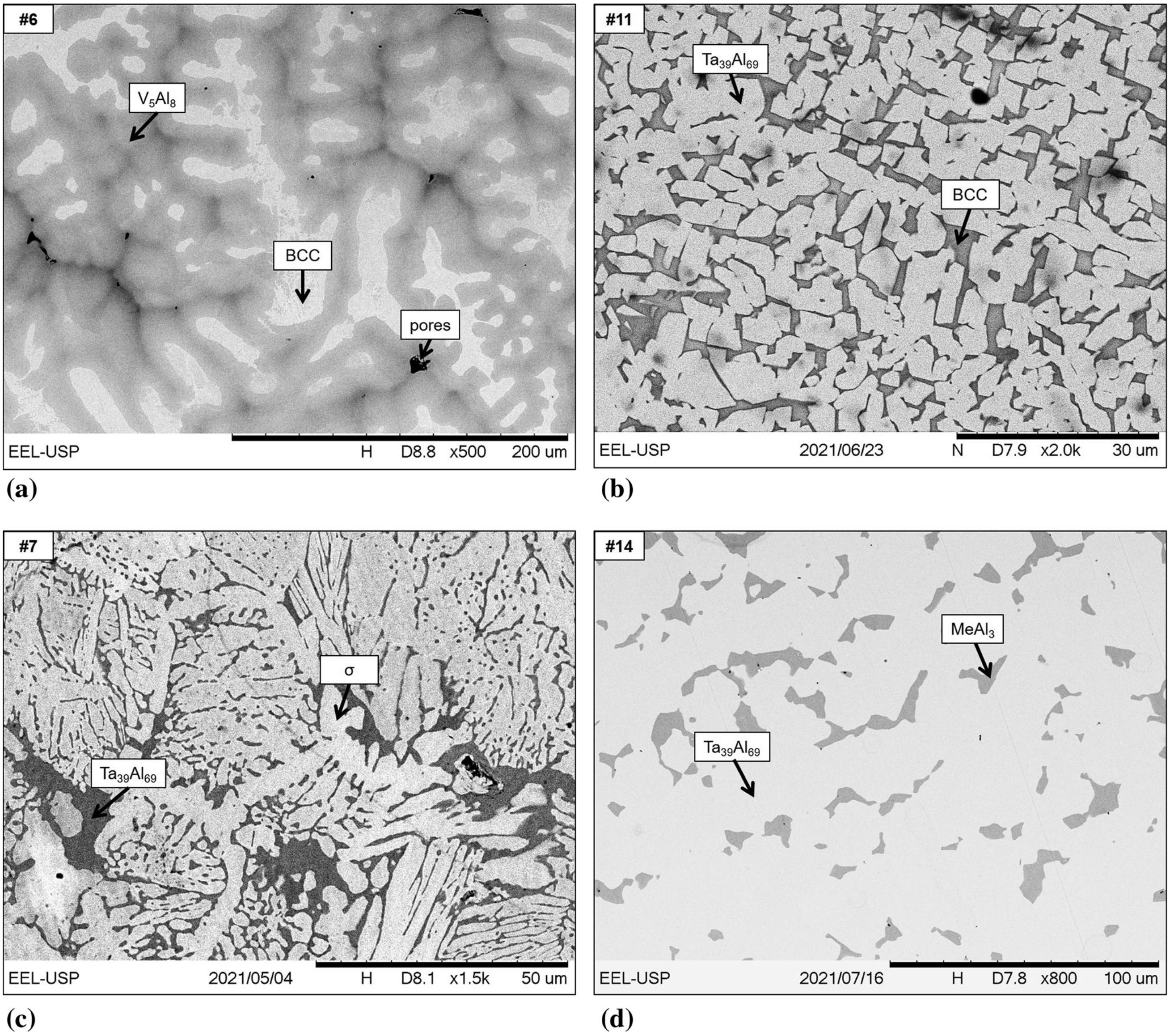

Fig. 4 Micrographs (SEM/BSE) of as-cast alloys in the BCC and σ primary solidification fields: (a) #6, (b) #11, (c) #7 and (d) #14

the possible composition deviations for each alloy according to calculations mentioned above. Symbols p^y represent liquid compositions of the peritectic invariant reactions from the binary systems (see Table 2 for details), while the symbols U, P and M correspond to class II, class III ternary invariant reactions and minimum point,

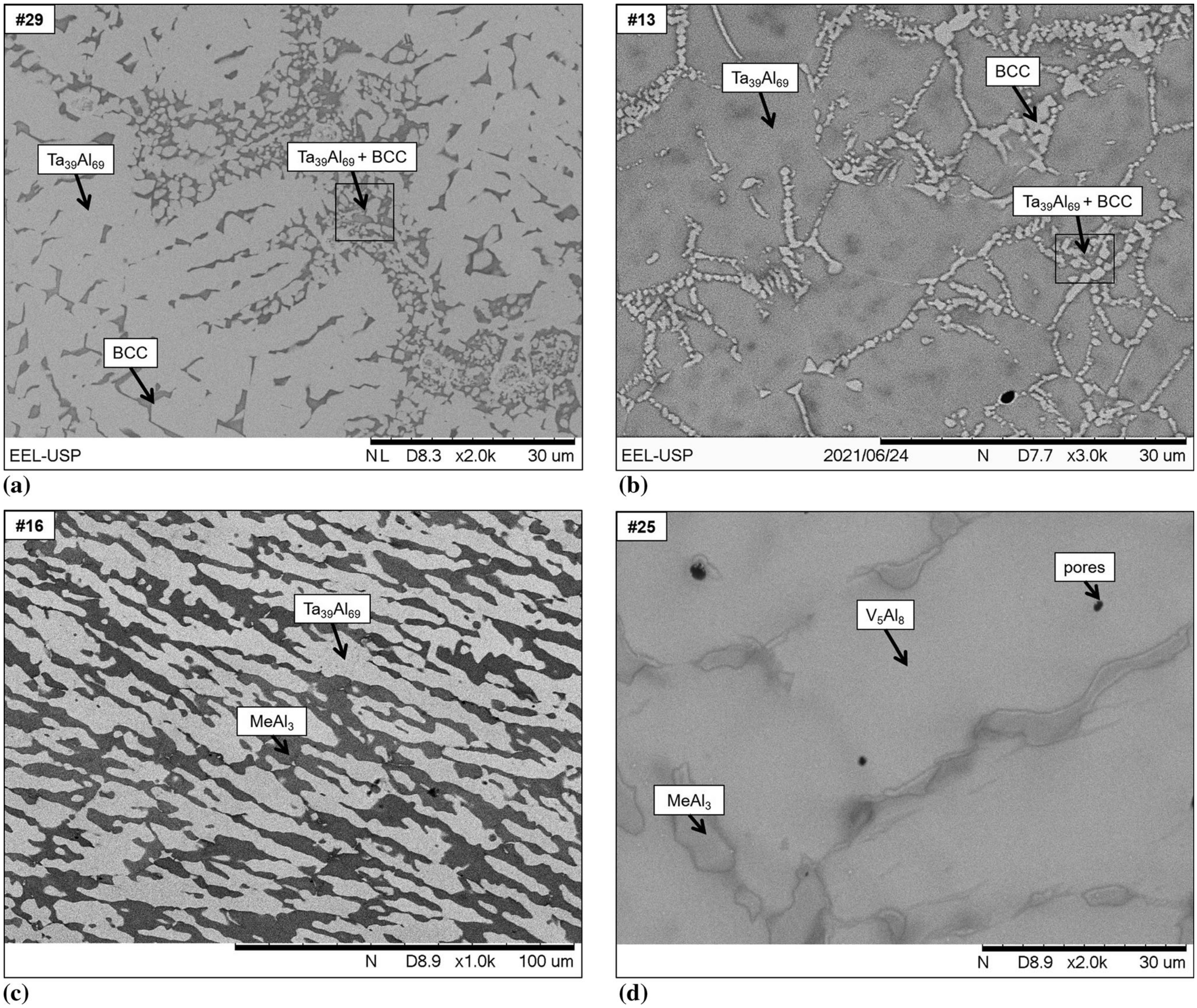

Fig. 5 Micrographs (SEM/BSE) of as-cast alloys in the $Ta_{39}Al_{69}$ and V_5Al_8 primary solidification fields: (a) #29, (b) #13, (c) #16, (d) #25

respectively. The arrows on the monovariant lines indicate the direction of decreasing temperature. The region with Al contents higher than 95 at.% was not investigated due to experimental difficulties. This region is reported based on thermodynamic extrapolation from well-established evaluations of binary subsystems using the Calphad approach.

Microstructural analyses (SEM/BSE, EDS and XRD) of as-cast alloys were used to determine the extents of the primary solidification fields of each phase as well as the nature of the monovariant lines and ternary invariant reactions. Although the isothermal sections at 1273 K reported by Raman and Bochvar[38,39] suggest an imiscibility of the isostructural compounds VAl_3 and (ε)-$TaAl_3$, phase separation was not observed in the as-cast microstructures. Thus, the solid solution formed by VAl_3 and (ε)-$TaAl_3$ in the present investigation is treated here as $MeAl_3$.

Alloys located in the primary solidification fields of BCC, $MeAl_3$, V_5Al_8, σ and $Ta_{39}Al_{69}$ were produced. BCC primary solidification field is dominant, which is in agreement with its large extent in the binary edges.[25,30,36] The presence of the ternary compound τ-$Al_{35-48}Ta_{32-42}V_{17-30}$ was not evidenced in the as-cast alloys, which is in agreement with the results obtained by Harbrecht et al.,[40] as explained in the section 2.2.

The nature of ternary invariant reactions (four class II and two class III) as well as their liquid phase compositions were estimated taking into consideration the microstructural features of the as-cast alloys and CALPHAD extrapolation based on data from Ref [25, 30, 36] (for

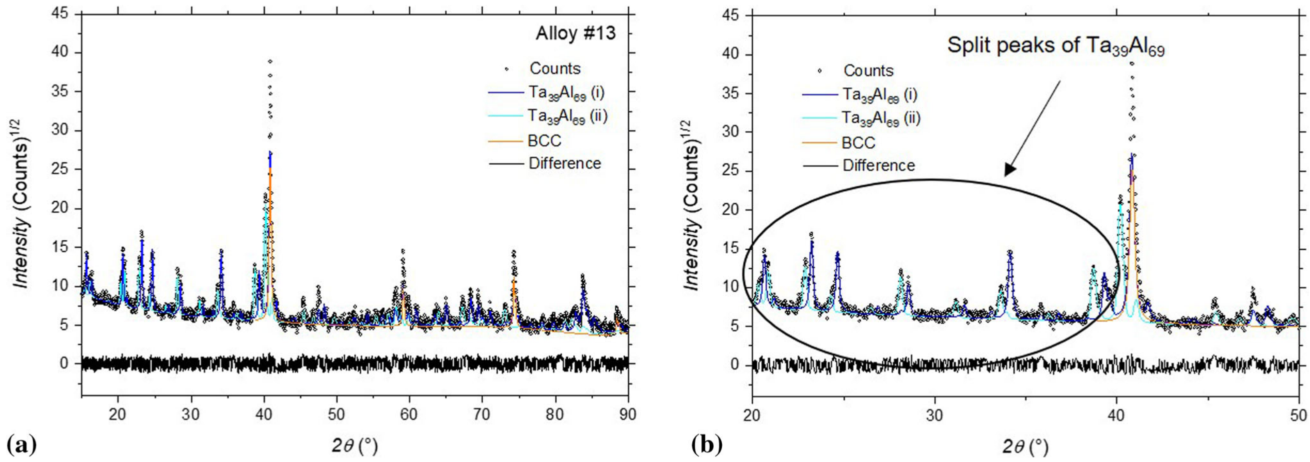

Fig. 6 X-ray diffractograms of as-cast alloy #13 (a) full range (b) details highlighting the split peaks at lower angles

reactions close to the Al corner, indicated in the left side of the Fig. 3).

These reactions are detailed in Table 4. The microstructural features of selected as-cast alloys will be discussed below, grouped in three different regions, to support the *liquidus* projection reported in Fig. 3.

4.1 The Ta-V Rich Region (BCC and σ Primary Solidification Regions)

Primary BCC phase was observed in the SEM/BSE micrographs of alloys #1-#6, #8-#9 and #12. Alloys #1-#5, #8-#9 and #12 solidified as BCC single-phase. No evidence of the ternary compound τ-$Al_{35-48}Ta_{32-42}V_{17-30}$ was found in the alloys (#1-#4, #8-#9 and #12) located close to its composition range based on the isothermal sections (see Fig. 2).

BCC primary phase surrounded by V_5Al_8 is observed in the SEM/BSE micrograph of alloy #6 shown in Fig. 4(a), suggesting its solidification path towards the p^4-P_I peritectic-type monovariant line. It is important to mention that V_5Al_8 shows a grey-contrast gradient, associated with the variation of its Al content as a function of temperature, which is consistent with the proposal for this phase in the Al-V system.

Simultaneous solidification of BCC together with $Ta_{39}Al_{69}$ was observed in the SEM/BSE micrograph of alloy #11, as shown in Fig. 4(b). Considering the morphology of these phases and the results discussed in the next section, the dark-grey regions are the BCC phase, while the polygonal light-grey regions are the $Ta_{39}Al_{69}$ phase. According to these results, the composition of alloy #11 is placed on the eutectic-type U_I-M_I monovariant line, Fig. 3.

Alloys #26 and #30 solidified as σ single-phase. Fig. 4(c) shows a SEM/BSE micrograph of alloy #7, containing primary σ phase surrounded by $Ta_{39}Al_{69}$, which confirms the peritectic nature of the p^2-U_I monovariant line. The same interpretation was adopted for alloy #10. The SEM/BSE micrograph of alloy #14 indicates only the presence of the $Ta_{39}Al_{69}$ and $MeAl_3$ phases, as observed in Fig. 4(d). However, some peaks from σ phase were identified in the XRD analyses, suggesting that its composition is located close to the p^2-U_I peritectic monovariant line. Thus, two consecutive peritectic reactions are suggested for this alloy composition.

4.2 The Intermediate Region ($Ta_{39}Al_{69}$ and V_5Al_8 Primary Solidification Regions)

Primary $Ta_{39}Al_{69}$ phase was observed in the microstructures of alloys #13, #15-#16, #18 and #31. Alloy #15 solidified as $Ta_{39}Al_{69}$ single-phase.

The SEM/BSE micrographs of alloys #29 and #13 are shown in Fig. 5(a) and (b), respectively. For both alloys, primary $Ta_{39}Al_{69}$ phase and an eutectic-type microconstituent formed by $Ta_{39}Al_{69}$ + BCC are observed. The BCC phase has a Ta content smaller than the primary $Ta_{39}Al_{69}$ phase in alloy #29, while it has a Ta content higher than the primary $Ta_{39}Al_{69}$ phase in alloy #13. These opposed solidification paths led us to suggest the presence of a minimum point indicated by M_I in Fig. 3, which may be connected to the congruent c^1 point from the Ta-V binary system. Thus, the solidification paths of alloys #27 and #29 move towards the U_I-M_I monovariant line, while the solidification paths of alloys #13, #28 and #31 move towards the P_I-M_I monovariant line. Moreover, split peaks of the $Ta_{39}Al_{69}$ phase were observed in the XRD results of these group of alloys (#13, #27-#29), which suggest a segregation effect in the $Ta_{39}Al_{69}$ primary solidification region. These split peaks are shown in the diffractogram of the alloy #13, Fig. 6.

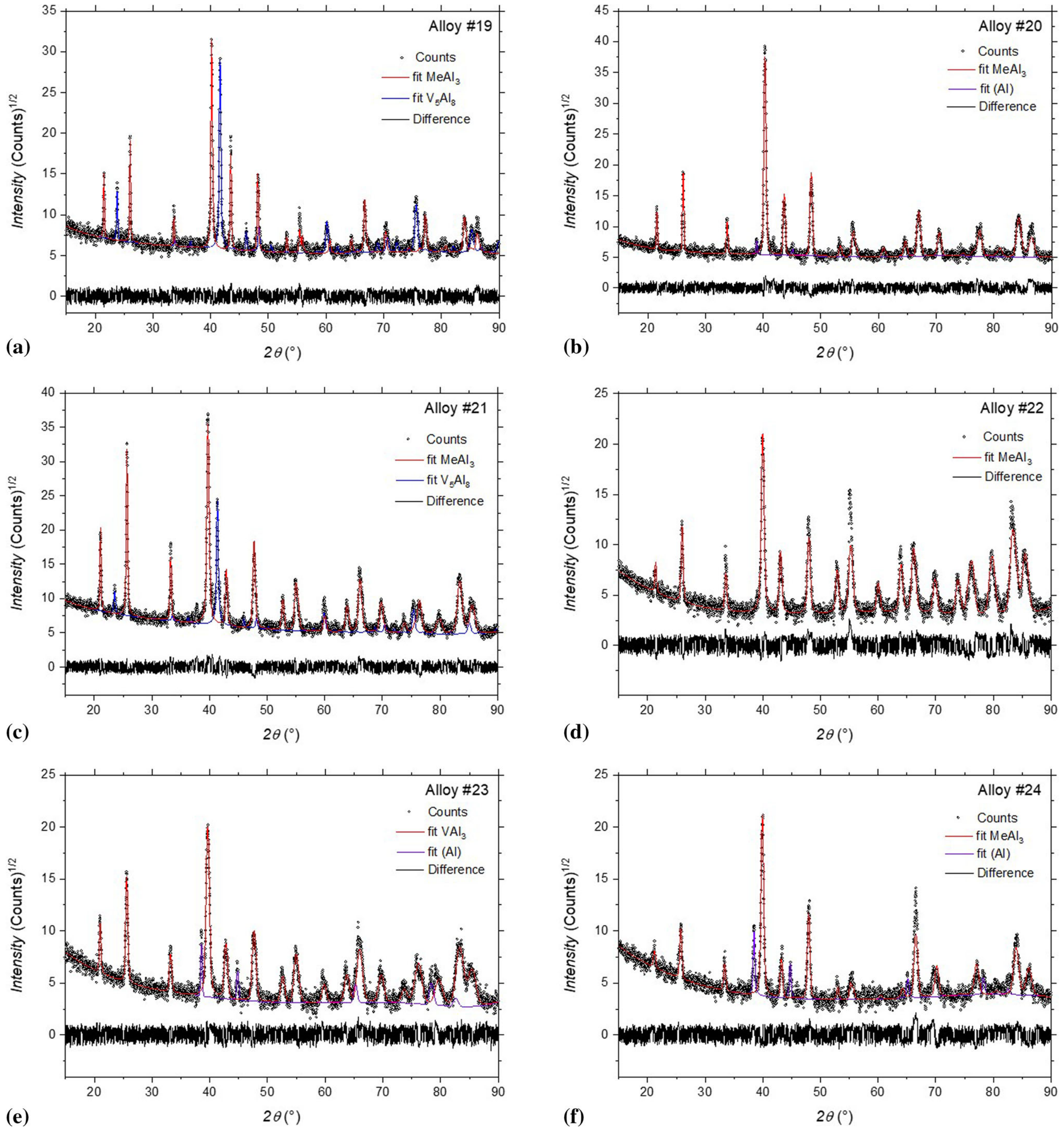

Fig. 7 XRD results of the as-cast alloys in the MeAl$_3$ primary solidification field: (a) #19, (b) #20, (c) #21, (d) #22, (e) #23 and (f) #24

The SEM/BSE micrograph of alloy #16, Fig. 5(c), shows the primary phase Ta$_{39}$Al$_{69}$ surrounded by MeAl$_3$, suggesting a solidification path towards the p^3-U$_{II}$ peritectic-type monovariant line.

Some peaks associated with the Ta$_{39}$Al$_{69}$ phase were observed by the XRD analysis of alloy #18, although its presence was not evidenced in the SEM/BSE micrographs. Furthermore, an eutectic-type microconstituent formed by MeAl$_3$ and V$_5$Al$_8$ was observed in the last solidification region. As discussed above, the p^3-U$_{II}$ monovariant line has a peritectic nature, which means that the liquid composition moves from Ta$_{39}$Al$_{69}$ primary solidification field towards the MeAl$_3$ primary solidification field. In addition, the compound Ta$_{39}$Al$_{69}$ was not observed to the alloys #17,

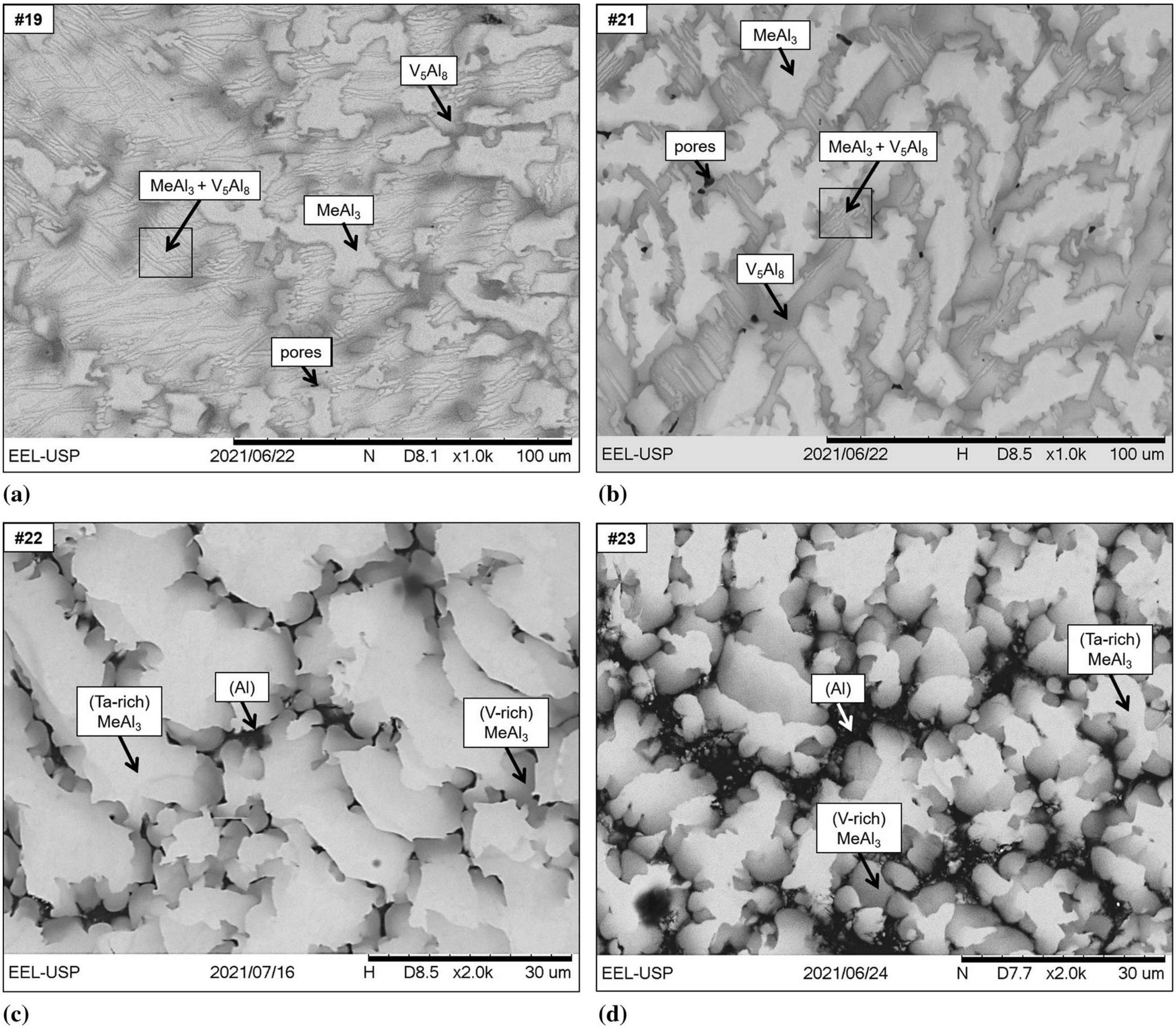

Fig. 8 Micrographs (SEM/BSE) of as-cast alloys in the $MeAl_3$ primary solidification field: (a) #19, (b) #21, (c) #22 and (d) #23

#19 and #21, which suggest that its composition (alloy #18) is near the p^3-U_{II} monovariant line.

Fig. 5(d) shows the SEM/BSE micrograph of alloy #25. After the primary solidification of V_5Al_8, a peritectic formation of $MeAl_3$ is observed in the last solidification region. Based on the EDS analyses, the $MeAl_3$ phase has a Ta composition smaller than that of the V_5Al_8 primary phase, suggesting that the solidification moves towards the Al-V binary side. The primary solidification field of V_5Al_8 is restricted to a small region close to the Al-V binary edge, as also observed in the *liquidus* projection of the Al-Nb-V,[8] which is similar to the present ternary system.

4.3 The Al-rich Corner ($MeAl_3$ Primary Solidification Region)

Due to experimental difficulties, the *liquidus* projection for Al contents higher than 95 at.% has not been addressed in this work. Therefore, no samples were produced to investigate the primary solidification of V_2Al_{21}, V_7Al_{45} and V_4Al_{23} phases. The construction indicated with dashed lines in Fig. 3 is tentative for this region (see the insert of Fig. 3 for details). The invariant reactions close to the Al-corner, as well as their compositions are indicated in Table 4, based on thermodynamic extrapolation using data from Ref [25, 30, 36].

Primary $MeAl_3$ phase was observed in alloys #17 and #19-24. Based on the experimental results obtained from SEM/BSE and XRD (see Fig. 7), no signs of phase separation between VAl_3 and (ε)-$TaAl_3$ were found.

Fig. 8(a) and (b) show the SEM/BSE micrographs of alloys #19 and #21. An enrichment of V content was observed from the center to the edge of the primary phase, while the Ta content decreased. The liquid composition reaches the U_{II}-p^5 monovariant line, when a eutectic-type microconstituent (formed by $MeAl_3$ and V_5Al_8) is solidified. In addition, the remaining liquid was transformed into V_5Al_8. The same solidification path was observed for the alloy #17. Comparing the solidification paths of these alloys with the microstructural data obtained for alloy #25, it is possible to suggest a change of nature of the U_{II}-p^5 monovariant line, (i.e. eutectic-type microstructures are solidified for compositions close to U_{II}, while peritectic-type microstuctures are solidified for compositions close to p^5). The transition of the nature in the U_{II}-p^5 may be placed between the compositions indicated by #19 and #20 in Fig. 3. This behavior was also observed in the *liquidus* projection of the Al-Nb-V[8] from the monovariant line between the $MeAl_3$ and V_5Al_8 primary solidification fields. Furthermore, the possible hypotheses of the presence of a maximum point at the U_{II}-p^5 is not consistent, since no sign of a class I reaction was observed in the microstructures of alloys #15, #18 and #19.

Primary $MeAl_3$ phase followed by peritectic formations of (Al) were observed in SEM/BSE micrographs of alloys #22 and #23, as exemplified in Fig. 8(c) and (d), respectively. The presence of the grey contrast in this primary phase corroborates the assumption of complete solubility in $MeAl_3$ structure. Moreover, the XRD results for these alloys, presented in Fig. 7, do not show split peaks resulting from the supposed phase separation.

5 Conclusion

Experimental results for the *liquidus* projection for the Al-Ta-V system are presented for the first time in the present work. Based on the microstructural characterization of thirty-one as-cast alloys via SEM/BSE, EDS and XRD, the *liquidus* projection of the Al-Ta-V system is reported. Five primary solidification regions were experimentally identified, with the BCC phase field filling most of the ternary system, as expected by the stability of this phase in the binary systems. The ternary phase τ-$Al_{35-48}Ta_{32-42}V_{17-30}$ was not found in the as-cast alloys. Two type II and one type III ternary invariant reactions are reported based on the experimental data. For Al contents higher than 99 at.%, two class II and one class III ternary invariant reactions are suggested based on extrapolated thermodynamic data from binary systems.

Acknowledgments The authors gratefully acknowledge the financial support from the Coordenação de Aperfeiçoamento de Pessoal de Nível Superior - Brasil (CAPES) - (Contract Number 88887. 605242/2021-00) and Conselho Nacional de Pesquisa (CNPq) - (Contract Number 161322/2021-2).

Conflict of interest The authors declare that they have no conflict of interest.

References

1. N. Stepanov, N. Yurchenko, D. Skibin, M. Tikhonovsky, and G. Salishchev, Structure and Mechanical Properties of the AlCrxNbTiV (x= 0, 0.5, 1, 1.5) High Entropy Alloys. J. Alloys Compd. **652**, 266–280 (2015)
2. O. Senkov, G. Wilks, D. Miracle, C. Chuang, and P. Liaw, Refractory High-Entropy Alloys. Intermetallics. **18**, 1758–1765 (2010)
3. S. Chen, X. Yang, K. Dahmen, P. Liaw, and Y. Zhang, Microstructures and Crackling Noise of AlxNbTiMoV High Entropy Alloys. Entropy **16**, 870–884 (2014)
4. E. Panina, N. Yurchenko, S. Zherebtsov, M. Tikhonovsky, M. Mishunin, and N. Stepanov, Structures and Mechanical Properties of Ti-Nb-Cr-V-Ni-Al Refractory High Entropy Alloys. Mater. Sci. Eng. A **786**, 139409 (2020)
5. L. Li, M. Li, M. Liu, B. Sun, C. Wang, J. Huo, W. Wang, and Y. Liu, Enhanced Oxidation Resistance of MoTaTiCrAl High Entropy Alloys by Removal of Al. Sci. China Mater. **64**, 223–231 (2021)
6. O. Senkov, S. Senkova, and C. Woodward, Effect of Aluminum on the Microstructure and Properties of Two Refractory High-Entropy Alloys. Acta Mater. **68**, 214–228 (2014)
7. J. Santos, N. Chaia, K. Borowski, A. Silva, D. Barros, D. Abreu, C. Nunes, and G. Coelho, Experimental Investigation of Phase Equilibria at 1200C in the Al-Nb-V System. J. Phase Equilibria Diffus. **41**, 172–180 (2020)
8. J. Santos, N. Chaia, K. Borowski, A. Silva, D. Barros, D. Abreu, C. Nunes, and G. Coelho, Liquidus Projection of the Al-Nb-V System. Calphad **71**, 102196 (2020)
9. J. Santos, A. Silva, P. Pires, T. Dorini, D. Barros, D. Abreu, L. Eleno, C. Nunes, and G. Coelho, Thermodynamic Modeling of the Al-Nb-V System. Calphad **74**, 102321 (2021)
10. D. Abreu, A. Silva, J. Santos, D. Barros, C. Barros, N. Chaia, C. Nunes, and G. Coelho, Liquidus Projection of the Al-Ti-Zr System. J. Alloys Compd. **849**, 156463 (2020)
11. D. Barros, J. Santos, D. Abreu, A. Silva, K. Borowski, N. Chaia, C. Nunes, and G. Coelho, Liquidus Projection of the Al-Cr-V System. J. Alloys Compd. **899**, 163258 (2021)
12. U.R. Kattner, The Thermodynamic Modeling of Multicomponent Phase Equilibria. JOM **49**, 14–19 (1997)
13. T. Kraft and Y.A. Chang, Predicting Microstructure and Microsegregation in Multicomponent Alloys. JOM **49**, 20–28 (1997)
14. A. Kroupa, Modelling of Phase Diagrams and Thermodynamic Properties Using Calphad Method—Development of Thermodynamic Databases. Comput. Mater. Sci. **66**, 3–13 (2013)
15. H.L. Lukas, S.G. Fries, and B. Sundman, *Computational Thermodynamics: The Calphad Method* (Cambridge University Press, 2007)

16. L. Hartsough and R. Hammond, The Synthesis of Low Temperature Phases by the CO-Condensation of the Elements: A New Superconducting A15 Compound, V3Al. Solid State Commun. **9**, 885–889 (1971)
17. V. Eremenko, Y. Natanzon, and V. Titov, Kinetics of Dissolution of Vanadium in Liquid Aluminum (Translation). Russ. Metall. **5**, 34–37 (1981)
18. D. Bailey, O. Carlson, and J. Smith, The Aluminium-Rich End of the Aluminium-Vanadium System. Trans. ASM. **51**, 1097–1102 (1959)
19. A. Ray, J. Smith, A Test for Electron Transfer in V4Al23. Acta Cryst. **13**, 876–884 (1960)
20. J.L. Murray, Al-V (Aluminum-Vanadium). Bull. Alloy Phase Diagr. **10**, 351–357 (1989)
21. N. Saunders, System Al-V, in *COST 507—Thermochemical Database for Light Metal Alloys*. ed. by I. Ansara, A.T. Dinsdale, M.H. Rand (Office for Official Publications of the European Communities, 1998), pp.95–98
22. K. Richter and H. Ipser, Al-V Phase Diagram Between 0 and 50 Atomic Percent Vanadium. Z. Metallkd. **5**, 383–388 (2000)
23. W.P. Gong, Y. Du, B.Y. Huang, R. Schmid-Fetzer, C.F. Zhang, and H.H. Xu, Thermodynamic Reassessment of the Al-V System. Z. Metallkd. **95**, 978–986 (2004)
24. B. Lindahl, X. Liu, Z. Liu, and M. Selleby, A Thermodynamic Re-assessment of Al-V Toward an Assessment of the Ternary Al-Ti-V System. Calphad **51**, 75–88 (2015)
25. A. Kroupa, M. Mazalová, and K. Richter, The Reassessment of the Al-V System and New Assessment of the Al-Si-V System. Calphad **59**, 47–60 (2017)
26. C. Danon and C. Servant, A Thermodynamic Evaluation of the Ta-V System. J. Alloys Compd. **366**, 191–200 (2004)
27. V. Eremenko, L. Tretyachenko, and R. Yakhimovich, Melt Diagram of the Tantalum-Vanadium System. Russ. J. Inorg. Chem. **5**, 1100–1112 (1960)
28. A.P. Nefedov, E.M. Sokolovskaya, A.T. Grigorev, I.G. Sokolova, and N.A. Nedumov, Solid State Phase Transformations in Vanadium-Tantalum Alloys. Russ. J. Inorg. Chem. **9**, 486–489 (1964)
29. J. Savitskii and E. Efimov, Superconducting Metallic Compounds and Their Alloys. Monatsh. Chem. **103**, 270 (1972)
30. J. Pavlů, X. Chen, and P. Rogl, Thermodynamic Modeling of Laves Phases in the Ta-V System: Reassessment Using First-Principles Results. Calphad **35**, 103–108 (2011)
31. Y. Du and R. Schmid-Fetzer, Thermodynamic Modeling of the Al-Ta System. J. Phase Equilibria **17**, 311–324 (1996)
32. P. Subramanian, D. Miracle, and S. Mazdiyasni, Phase Relationships in the Al-Ta System. Metall. Trans. A **21**, 539–545 (1990)
33. S. Mahne, F. Krumeich, and B. Harbrecht, Phase Relations in the Al-Ta System: On the Translational Symmetries of Al3Ta2 and AlTa. J. Alloys Compd. **201**, 167–174 (1993)
34. A. Nowotny and H. Neckel, Chemical Bonding in Interstitial Compounds. J. Inst. Met. **97**, 161–164 (1969)
35. S. Meschel and O. Kleppa, Standard Enthalpies of Formation of 5d Aluminides by High-Temperature Direct Synthesis Calorimetry. J. Alloys Compd. **197**, 75–81 (1993)
36. V. Witusiewicz, A. Bondar, U. Hecht, J. Zollinger, V. Petyukh, O. Fomichov, V. Voblikov, and S. Rex, Experimental Study and Thermodynamic Re-assessment of the Binary Al-Ta System. Intermetallics **18**, 92–106 (2010)
37. A. Belsky, M. Hellenbrandt, V. Karen, and P. Luksch, New Developments in the Inorganic Crystal Structure Database (ICSD): Accessibility in Support of Materials Research and Design. Acta Crystallogr. Sect. B Struct. Sci. **58**, 364–369 (2002)
38. A. Raman, Röntgenographische Untersuchungen in einigen T-T5-Al systemen. Z. Metallkd. **57**, 535–540 (1966)
39. N.R. Bochvar, Aluminium-Tantalum-Vanadium, in *Ternary Alloys*, vol. 8, p 409–411, VCH, 1993
40. B. Harbrecht, N. Rheindorf, and V. Wagner, τ-Al2.9Ta2.7V1.4, A New Type of Pentagonal Antiprismatic Columnar Structure. J. Alloys Compd. **234**, 6–11 (1996)